Construction on Morphology of Aquatic Animals via Moving Least Squares Method

Chee Kin Cheah[1] and Wah Yen Tey[1,2,*]

[1] Department of Mechanical Engineering, Faculty of Engineering, UCSI University, Kuala Lumpur, Malaysia
[2] Malaysia-Japan International Institute of Technology, Universiti Teknologi Malaysia, Kuala Lumpur, Malaysia

* Email: teywy@ucsiuniversity.edu.my

Abstract. Unmanned underwater vehicle (UUV) is an effective instrument to allow human to execute hazardous underwater mission without being exposed to life risk. Recently, UUV has gained increased popularity in the field of oceanography, underwater archaeology, underwater cable examination, military usage and hydrodynamic survey operation. Since aquatic animals have great capability to circumvent the drag underwater for efficient swimming compared with the torpedo-like man-made submarine, the morphology of aquatic animals shall be investigated in order to improve the efficiency of UUV. However, the complexity and non-linearity of their body shapes has hindered the formation of its morphological equations. Hence, this research aims to apply the mathematical model of moving least squares method to construct continuous equations which describe the bionic body shape of batoid and dolphin. The work will render geometrical support for computer-aided design and fluid dynamics analysis in the future.

1. Introduction

Unmanned underwater vehicles (UUV) are mechanical devices which can be controlled to perform underwater missions such as path following [1], navigation sensing [2] and oceanography mapping [3], without human occupant. The hydrosphere is covering 70% of the earth, while 97% of the hydrosphere is made-up from the ocean, leaving around 3% from the fresh water [4]. It is almost impossible to explore the entire underwater environment with submersibles. In order to discover the hidden world beneath the sea level, the UUV plays its imperative role by disencumbering human from the hazardous underwater missions [5]. Indeed, UUV has been a valuable tool for underwater exploration and operation, in tandem with the growing importance of ocean [6].

The first prototype of the UUV was built in 1957, and it was used for diffusion investigation, acoustic transmission studies and submarine wakes research [7,8]. With increasing interest and curiosity toward the underwater world, humans intensifies the investment in the invention and modification of UUV. Due to its lower cost and smaller size compared to the large expensive submarines, UUV appears to be more promising in term of manufacturing cost and operating agility [9,10].

Evolution of the aquatic animals has taken place since millions of years ago and they spent their entire life in the viscous medium. The water drag, form drag and induced drag are the main swimming resistances for the aquatic animals [11]. Water drag refers to the viscous frictional force between the water contact surface and body surface. Form drag refers to the resistance force to displace the water from one particular place to another, while induced drag refers to the energy lost in vortices created at

fins during swimming. Since the aquatic animals are regarded to be having great capability to circumvent the drag underwater for efficient swimming [12], the morphologies of aquatic and marine animals are studied in order to improve the efficiency of UUV [13]. Discovery of the aquatic animals' morphology has sparked the interests of engineers to invent swimming machines which mimic the shape of aquatic animals, such as the biomimetic fins and divers' flippers [14,15]. Swimming efficiency of aquatic animals are generally ranging from 80% to 90%, but the average efficiency of the manmade thruster is not more than 50% [16]. The naturally streamlined body curvature and locomotion patterns of these aquatic animals are rendering the ideal models to be readily applied in UUV design.

In fact, aquatic animals often possess unique and complex curvature for their body shape that allows them to swim or propel underwater in swift and smooth locomotion. Unfortunately, most of the current designs are based on a very rough approximation of fish morphology, possibly due to the lack of detailed mathematical information of its geometry. In this paper, equations were constructed to describe the 3D geometry of aquatic animals. Our work focuses on the geometry of body surface of rajiform batoid and common dolphin. Moving least squares method [17] has been applied as the mathematical tool for the geometry construction. The generated equations is expected to benefit the oceanic engineering communities in the future, such as for fluid dynamics analysis and computer-aided design (CAD).

2. Methodology

2.1 Mathematical Modelling of Moving Least Squares Method

Moving Least Square (MLS) is a method to approximate and construct a continuous function for a set of disordered data or scattered sampling points [18]. It has wide applications in geometry formation [19], image processing [20] and solution of meshfree techniques [21], due to its robustness in generating a continuous equation to connect most of the irregular sampling data [17,22]. There are a lot of researchers and scholars have been utilise MLS for optimisation studies and engineering analysis [17,23,24]. This method is able to connect all of the disordered plots with quasi-interpolation, eventually generating an approximated smooth surface curve. This method is able to reconstruct a smooth 3D surface in CAD or digital graphic design.

Let the data set of z_i which can be represented by the approximated function z^h:

$$z^h = P_1 a_1 + \cdots + P_m a_m = \sum_{j=1}^{m} P_j a_j \tag{1}$$

where P is the guess variables of function (parabolic function basically), a is its associating coefficients (constant values), while m is the maximum number of guess function applied. The difference between the actual value (z) and approximated value (z^h) is the error (R). In MLS method, the weighted discrete norms, J can formed as:

$$J = \sum_{i=1}^{n} W_i \left(z^h{}_i - z_i \right)^2 = \sum_{i=1}^{n} W_i \left(\sum_{j=1}^{m} P_j a_j - z_i \right)^2 \tag{2}$$

The minimisation of J is then conducted such that:

$$\frac{\partial J}{\partial a} = 0 \tag{3}$$

The differential products of J are combined as summation term and rearranged as a matrix form of $Aa = B$, and therefore the coefficients a can be identified as in Eq. (4):

$$a = A^{-1}B \tag{4}$$

where:

$$a = \begin{bmatrix} a_1 & a_2 & \cdots & a_m \end{bmatrix}^{\mathrm{T}}$$

$$A = \sum_{i=1}^{m} W_i \mathbf{P}(x_i) \mathbf{P}(x_i)^{\mathrm{T}}$$

$$\mathbf{P}(x_i) = \begin{bmatrix} P_1(x_i) & P_2(x_i) & \cdots & P_m(x_i) \end{bmatrix}^T$$

$$B = \begin{bmatrix} \Sigma W_i(P_1)_i z_i & \Sigma W_i(P_2)_i z_i & \cdots & \Sigma W_i(P_m)_i z_i \end{bmatrix}^T$$

There are many weight functions available [25], yet quartic spline function is chosen due to its simplicity and convenience:

$$W = \begin{cases} 1 - 6r_i^2 + 8r_i^3 + 3r_i^4 & 0 \le r_i \le 1 \\ 0 & r_i \ge 1 \end{cases} \tag{5}$$

where:

$$r_i = \frac{\left| \sqrt{(x - x_i)^2 + (y - y_i)^2} \right|}{\left| \sqrt{(x_{max} - x_{min})^2 + (y_{max} - y_{min})^2} \right|} \tag{6}$$

(x,y) is the sampling point (any fixed point in the problem domain), while x_i and y_i are the x- and y-component coordinate points available throughout the domain. x_{max}, x_{min}, y_{max} and y_{min} refers to the maximum coordinate at x-component domain, mininum coordinate at x-component domain, maximum coordinate at y-component domain, minimum coordinate at y-component domain, respectively.

2.2 Data Sampling

Before collecting a set of data, the computed tomography (CT) of a rajiform batoid (*Dasyatis Sabina*) is obtained from the work of Fontanella et al. [26], as shown in Figure 1. The CT scans of the rajiform batoid are applied with gridlines according to their real scale, where it is 1 cm per grid. Figure 2 used to observe and determine the set of coordinates for animal's geometry.

Figure 1. CT scan of a rajiform batoid, *Dasyatis Sabina* adapted from the work of Fontanella et al. [26] in (a) side view and (b) dorsal view.
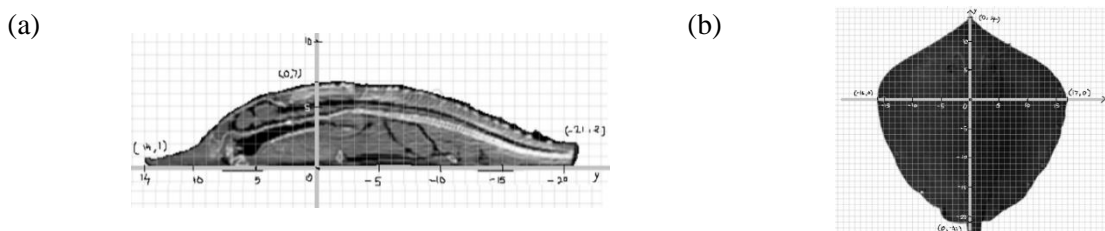

Figure 2. Gridlines was applied on the CT scan of a rajiform batoid, *Dasyatis Sabina* adapted from the work of Fontanella et al. [26] in (a) side view and (b) dorsal view.

On the other hand, the CAD drawing of a common dolphin (*bottlenose dolphin*) is obtained, as shown in Figure 3. The CT scans of the common dolphin (Figure 4) are obtained to further support the data collection of the dolphin's geometry [27]. The CAD drawing of a common dolphin (*bottlenose dolphin*) is applied with gridlines accordingly. Knowing that the average total length of an adult dolphin is around 230 cm and the largest diameter is around 60 cm [28], the gridlines split the figure with 1:10 ratio, in which every single grid is equivalent to 10 cm.
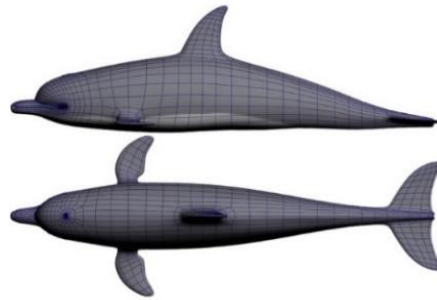
Figure 3. CAD drawing of a common dolphin (side & dorsal view) is retrieved from Maya Tutorials.

Figure 4. CT scan of a common dolphin (side view) is adapted from [27].

2.3 Data Collection

The selected samples outline the back bone of a batoid, body frame and the frame of the disc-shaped pectoral fin, as shown in Figure 5. Microsoft Excels is used to record the data and estimate the remaining of the coordinates around the body of the batoid by assuming each section of body is a semi-circle with respect of y-axis, where:

$$r^2 = x^2 + z^2 \quad , \quad -r \leq x \leq r \quad \& \quad r = z_{max} \quad at \quad y = 0,1,2,\dots$$

By rearranging it,

$$z = \sqrt{r^2 - x^2} \quad , \quad -r \leq x \leq r \quad \& \quad r = z_{max} \quad at \quad y = 0,1,2,\dots$$

where z_{max} is the maximum points in z-component domain. The completed reference plot that readily serves as an initial input to the moving least square matrix is shown in Figure 5(a), while the surface plot is shown in Figure 5(b).

Similarly, the samples of coordinates of dolphin are collected from the model as illustrated in Figure 6(a) and (b). The completed reference plots for top-half and bottom-half of a common dolphin's body are readily serves as an initial input to the moving least square matrix. The surface plot according to reference points as in Figure 6(a) and (b) is plotted into Figure 6(c) and (d) respectively.
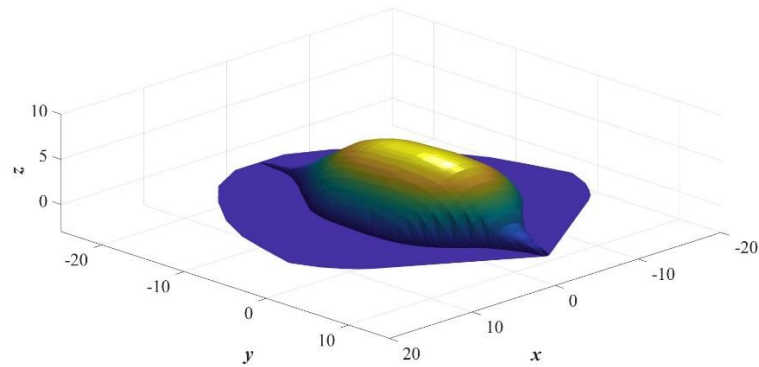
(a)
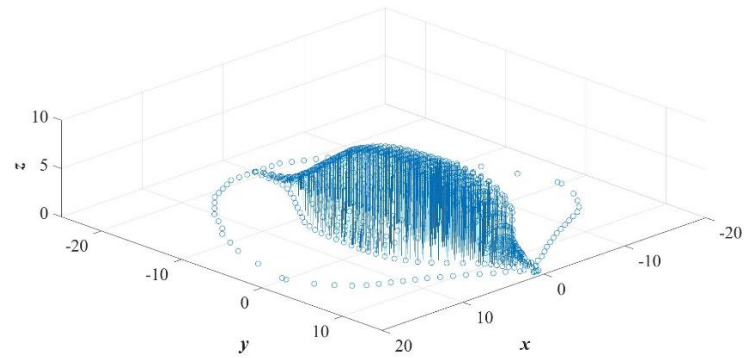
(b)

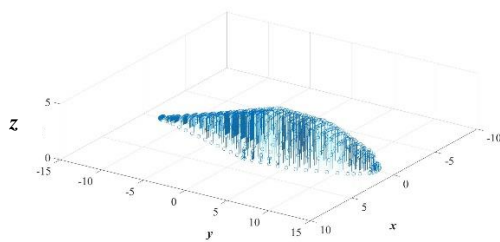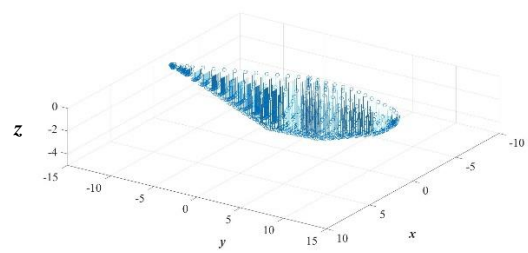**Figure 5.** (a) Reference plot which resembles of a rajiform batoid; (b) surface plot according to the reference plot of a rajiform batoid.

(a)   (b)
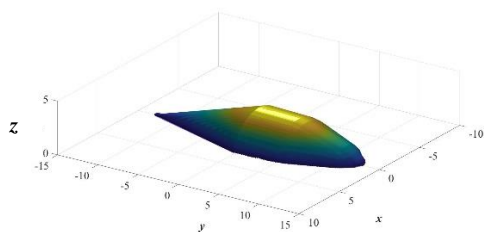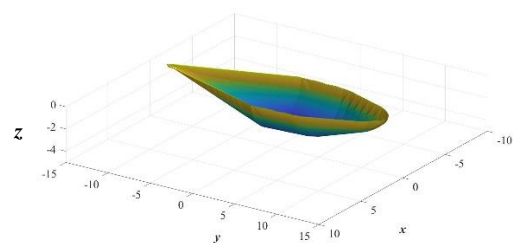
(c)   (d)

Figure 6. (a) Reference plot resembles of a dolphin's body (upper part); (b) reference plot resembles of a dolphin's body (lower part); (c) surface plot according to the reference plot of a dolphin's body (upper part); (d) surface plot according to the reference plot of a dolphin's body (lower part).

3. Result and Discussions

The surfaces formed from initial reference plots, as shown in Figure 5(a), Figures 6(a) and 6(b), might not as similar as the geometry of the real aquatic animals. However, the focus of our work, to enhance the dimensional continuity for the geometry boundaries and its surfaces. The coordinates around the surfaces are estimated by assuming as if they are circles which are perpendicular along the y-axis. MLS solver serves the main purpose to reconstruct a continuous equation according to the data input from the initial reference plots. Since coordinate on z-axis in every 3D geometry equations are closely related to the coordinate on x-axis and y-axis, the z-point can be described as a combination of variable x and y. The guess function is tuned by trial and error for the best possible results that we can obtain.

For the rajiform batoid, the coefficient for each variable is determined using the MLS solver that we developed using MATLAB. The approximated equation for the batoid surface can be illustrated as in Eq. (7).

$$z_{\text{batoid}} = 7.25 - 0.7\left[7 - \exp\left(2 - 0.05x^2 - 0.000167y^4\right)\right] - 0.15y - 0.0136x^2 - 0.006y^2 + 0.0006xy^2$$

$$+ 0.0001yx^2 + 0.0004y^3 + 0.0026\cos\left(20|x|\right)\cos\left(20|y|\right) + 0.0445\sin\left(20|x|\right)\sin\left(20|y|\right) \tag{7}$$

Graphical plots for Eq. (7) can be demonstrated in Figure 7. Figure 7(a) indicates the approximated reference plot of a rajiform batoid formed from MLS solver, while Figure 7(b) shows an approximated smooth surface curvature that resembles a rajiform batoid.
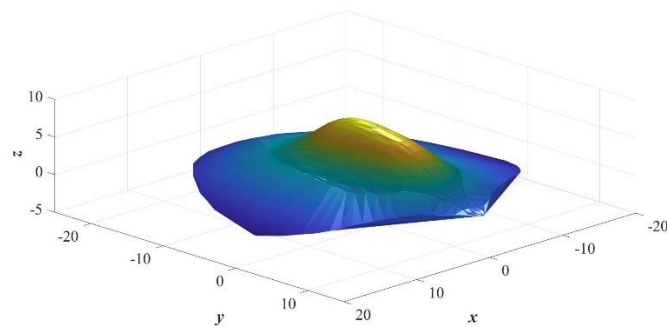
(a)
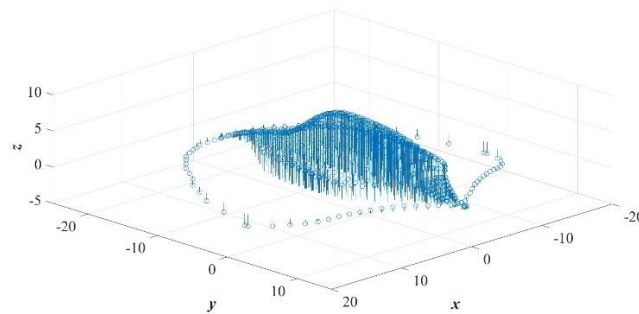
(b)

Figure 7. (a) Approximated reference plot of a rajiform batoid generated from Eq. (7); (b) approximated surface plot of a rajiform generated from Eq. (7).

The location difference contour comparing the z-component coordinate between reference points (Figure 5(a)) and approximated points (Figure 7(a)) is plotted in Figure 8. The value of Root Mean Square Error (RMSE) is 0.8843, which is small enough to justify Eq. (7). RMSE can be calculated as:

$$\text{RMSE} = \sqrt{\frac{\Sigma\left(z - z_{batoid}\right)^2}{n}} \tag{8}$$

The highest difference can be observed on the inflated bone side and the flattened wings of the batoid. With credits to these differences, the surface of the generated batoid is smoother compared with the refereed batoid as in Figure 5(b). The batoid generated as in Figure 7(b) has a more "naturally streamlined" surface shape, making it to be closer to bionic morphology of batoids.
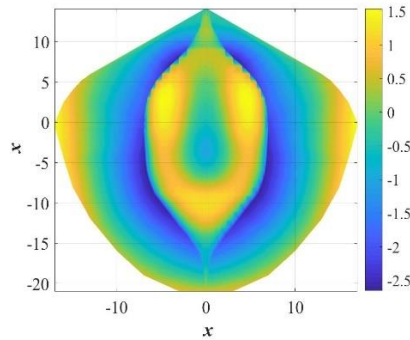

Figure 8. Location difference contour plot in comparing z-component coordinate of the reference coordinate and approximated coordinate.

For the common dolphin, the coefficient for each variable is determined with the MLS solver as well. In the case of dolphin, the body shape is known to be a torpedo shape, or a shape form with many circles with different diameter along the y-axis. Due to the limitation of MLS, the common dolphin's body has to be plotted separately as top-half and bottom-half, as shown in Figure 6. The pectoral limbs, dorsal fin, and caudal limbs are not included in the plots in order to obtain greater accuracy of curvature for the body.

The approximated equations for upper part and lower part of dolphin have been formulated respectively in Eq. (9) and (10).

$$z_{\text{batoid}} = 2.9 + 0.14y - 0.29x^2 - 0.174y^2 - 0.0035yx^2 + 0.0008y^3 + 0.0098\cos\left(20|x|\right)\cos\left(20|y|\right) \qquad (9)$$

$$z_{\text{batoid}} = -2.9 - 0.14y + 0.29x^2 + 0.174y^2 + 0.0035yx^2 - 0.0008y^3 - 0.0098\cos\left(20|x|\right)\cos\left(20|y|\right) \quad (10)$$

From Eqs. (9) and (10), the approximated reference plot and surface plot of a common dolphin's body can be computed in Figure 9.

The approximated reference and surface plots as obtained in Figure 9 are close to the observation on Figure 6. The RMSE for dolphin plot is 0.2424, which is much lower compared with the batoid's, possibly due to its simpler geometry without high gradient along its surface. The location difference contour for dolphin study has been plotted in Figure 10. The greatest difference can be observed around the highly deforming section of the torpedo-like body of dolphin.

In general, MLS computation could produce the surface plots which have obvious smoother curvature than the initial reference plots. Indeed, MLS encounters its limitation in 3D plotting of data, such that the coordinates in the data sample cannot be overlapping (i.e. more than one values of z within similar x and y coordinate). Therefore, the modelling for common dolphin's body has to be separated into two parts. MLS solver has a better precision only if the studied body is a uniform curvature. Thus, dolphin's dorsal fin, caudal limbs, pectoral limbs and the tail of batoid has to be neglected and removed from the main body if a more accurate result is desired. The variables have to be manipulated wisely in order to generate a better continuous equation.
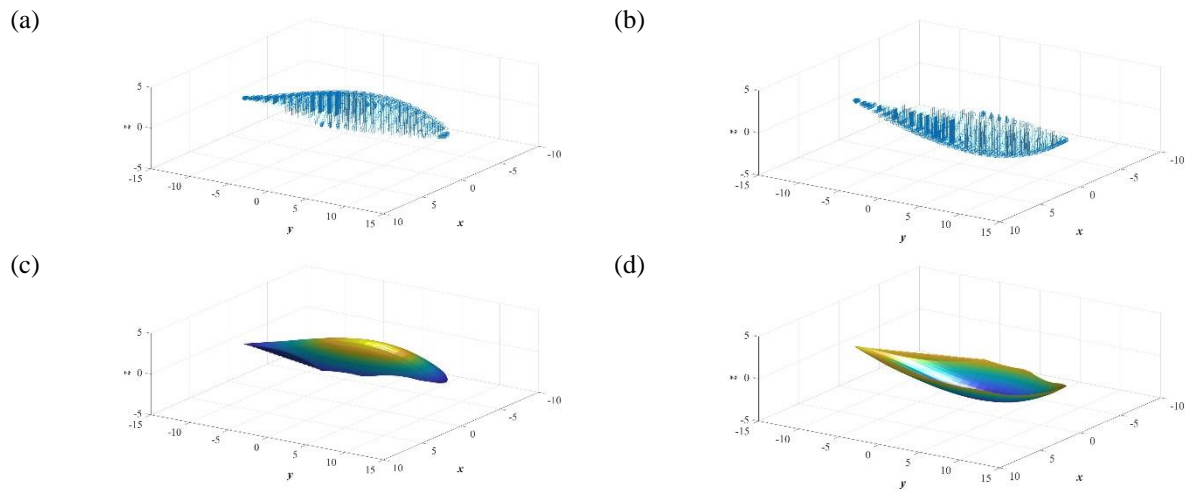
(a)   (b)

(c)   (d)

Figure 9. (a) Approximated reference plot resembles of a dolphin's body (upper part); (b) approximated reference plot resembles of a dolphin's body (lower part); (c) approximated surface plot according to the reference plot of a dolphin's body (upper part); (d) approximated surface plot according to the reference plot of a dolphin's body (lower part).
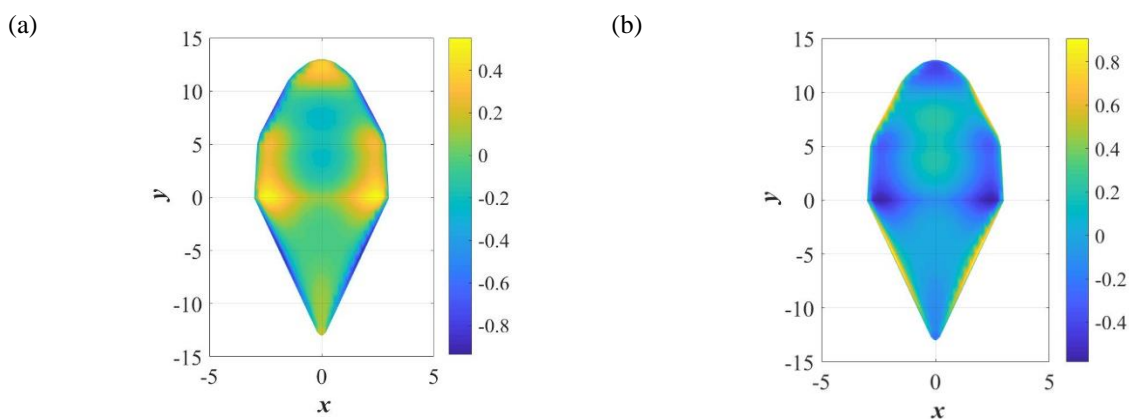
(a)   (b)

Figure 10. Location difference contour plot in comparing z-component coordinate of the reference coordinate and approximated coordinate for (a) upper part of dolphin; and (b) lower part of dolphin.

4. Conclusion

In conclusion, continuous equations which describe the morphology of rajiform swimmer (batoid) and common dolphin have been constructed using MLS. Although the input data is not exactly the same with the real geometry of the selected aquatic animals, the MLS solver is still able to generate surfaces with smoother appearance. The coefficients of each variable are identified in the process after setting the possible variables and inserting a set of 3D coordinates. The proposed equations in this study would provide geometrical input for computer-aided design (CAD) and fluid dynamics analysis in the future.

Acknowledgment

References

[1]   Lapierre L and Jouvencel B 2008 Robust nonlinear path-following control of an AUV *IEEE J. Ocean. Eng.* **33** 89–102

[2]   Yan Z, Wang L, Wang T, Yang Z, Chen T and Xu J 2018 Polar cooperative navigation algorithm for multi-unmanned underwater vehicles considering communication delays *Sensors (Switzerland)* **18**

[3]   Chen E and Guo J 2014 Real time map generation using sidescan sonar scanlines for unmanned underwater vehicles *Ocean Eng.* **91** 252–62

[4]   Gregory K, Simmons I, Brazel A, Day J, Keller E, Sylvester A and Yáñez-Arancibia A 2014 Hydrosphere *Environ. Sci. A Student's Companion* 121–2

[5]   Kyo M, Hiyazaki E, Tsukioka S, Ochi H, Amitani Y, Tsuchiya T, Aoki T and Takagawa S 2002 The sea trial of "KAIKO", the full ocean depth research ROV pp 1991–6

[6]   Bian J and Xiang J 2018 QUUV: A quadrotor-like unmanned underwater vehicle with thrusts configured as X shape *Appl. Ocean Res.* **78** 201–11

[7]   Jain S K, Mohammad S, Bora S and Singh M 2019 A Review Paper on: Autonomous Underwater Vehicle **6** 4–7

[8]   Kadir A M A, Kasno M A, Aras M S M, Tumari M Z M and Saat S 2018 Fuzzy logic controller design for autonomous underwater vehicle (Auv)-yaw control *ARPN J. Eng. Appl. Sci.* **13** 1608–14

[9]   Niu H, Adams S, Husain T, Bose N and Lee K 2009 Applications of Autonomous Underwater Vehicles in Offshore Petroleum Industry Environmental Effects Monitoring Memorial University of Newfoundland

[10]   Asakawa K, Kojima J, Kato Y, Matsumoto S and Kato N 2000 Autonomous underwater vehicle AQUA EXPLORER 2 for inspection of underwater cables *Proceedings of the 2000 International Symposium on Underwater Technology, UT 2000* pp 242–7

[11]   Sfakiotakis M, Lane D M and Davies J B C 1999 Review of fish swimming modes for aquatic locomotion *IEEE J. Ocean. Eng.* **24** 237–52

[12]   Tey W Y and Azwadi C S N 2015 A Review: The Development of Flapping Hydrodynamics of Body and Caudal Fin Movement Fishlike Structure *J. Adv. Rev. Sci. Res.* **8** 19–38

[13]   Pacholak S and Brücker C 2017 Size does matter: The use of fish motion for improving human swimming simulations *Appl. Math. Model.* **46** 339–53

[14]   Alam K, Ray T and Anavatti S G 2014 Design and construction of an autonomous underwater vehicle *Neurocomputing* **142** 16–29

[15]   Salazar R, Fuentes V and Abdelkefi A 2018 Classification of biological and bioinspired aquatic systems: A review *Ocean Eng.* **148** 75–114

[16]   Zhou C and Low K H 2010 Better endurance and load capacity: An improved design of manta ray robot (RoMan-II) *J. Bionic Eng.* **7**

[17]   Lancaster P and Salkauskas K 1981 Surfaces generated by moving least squares methods *Math. Comput.* **37** 141–58

[18]   Garimella R V 2017 *A Simple Introduction to Moving Least Squares and Local Regression Estimation*

[19]   Cao F and Li M 2015 Spherical data fitting by multiscale moving least squares *Appl. Math. Model.* **39** 3448–58

[20]   Lee Y J and Yoon J 2015 Image zooming method using edge-directed moving least squares interpolation based on exponential polynomials *Appl. Math. Comput.* **269** 569–83

[21]   Felter C L, J. H. Walther and C. Henriksen 2014 Moving least squares simulation of free surface flows *Comput. Fluids* **91** 47–56

[22]   LU Y 2016 A meshless method based on moving least squares for the simulation of free surface flows *J. Zhejiang Univ. Sci. A* **17** 130–43

[23]   Duflot M and Nguyen-Dang H 2002 A truly meshless Galerkin method based on a moving least

squares quadrature *Commun. Numer. Methods Eng.* **18** 441–9

[24]   Zhang L, Gu T, Zhao J, Ji S, Hu M and Li X 2013 An improved moving least squares method for curve and surface fitting *Math. Probl. Eng.* **2013**

[25]   Liu G R 2018 Meshfree Shape Function Construction *Meshfree Methods - Moving Beyond the Finite Element Method*

[26]   Fontanella J E, Fish F E, Barchi E I, Campbell-Malone R, Nichols R H, DiNenno N K and Beneski J T 2013 Two- and three-dimensional geometries of batoids in relation to locomotor mode *J. Exp. Mar. Bio. Ecol.* **446** 273–81

[27]   Ivančić M, Solano M and Smith C R 2014 Computed tomography and cross-sectional anatomy of the thorax of the live bottlenose dolphin (Tursiops truncatus) *Anat. Rec.* **297** 901–15

[28]   Lockyer C 2003 Dolphins, porpoises and whales of the world. The IUCN red data book *Biol. Conserv.* **61** 146–7